Supplementary information

Tip Dependence of Three-Dimensional Scanning Force Microscopy Images of Calcite-Water Interfaces Investigated by Simulation and Experiments

Keisuke Miyazawa,[ab] John Tracey,[c] Bernhard Reischl,[de] Peter Spijker,[c] Adam S. Foster,[ac] Andrew L. Rohl,[f] and Takeshi Fukuma*[ab]

[a] *Division of Electrical Engineering and Computer Science, Kanazawa University, Kakuma-machi, Kanazawa 920-1192, Japan. E-mail: fukuma@staff.kanazawa-u.ac.jp*
[b] *Nano Life Science Institute (WPI-NanoLSI), Kanazawa University, Japan.*
[c] *COMP Centre of Excellence, Department of Applied Physics, Aalto University, Helsinki FI-00076, Finland. E-mail: adam.foster@aalto.fi*
[d] *Institute for Atmospheric and Earth System Research/Physics, Faculty of Science, University of Helsinki, PO Box 64, FI-00014, Finland.*
[e] *Curtin Institute for Computation, Curtin University, P.O. Box U1987, Perth, Western Australia 6845, Australia.*
[f] *Curtin Institute for Computation and School of Electrical Engineering, Computing and Mathematical Sciences, Curtin University, P.O. Box U1987, Perth, Western Australia 6845, Australia.*

1 3D-SFM Measurements and Data Processing

Figure S1 shows the principle of a 3D-SFM measurement and the procedure for the conversion from the measured 3D frequency shift (Δf) image to a 3D force (F) image. In 3D-SFM, the tip is laterally scanned in the same way as in the conventional FM-AFM. At the same time, tip is also vertically scanned with a fast sinusoidal wave (Fig. S1a). During the 3D tip scanning, Δf induced by the interaction force applied to the tip is recorded to produce a 3D Δf image with subnanometer-scale resolution (Fig. S1b).

We processed the measured 3D Δf images as previously reported in detail in [1]. Here, we only explain it in short. Generally, the experimentally obtained 3D Δf image are distorted by various factors such as linear/nonlinear mechanical drifts and electrical noises. To remove some of the distortions, we applied linear drift corrections and a correlation averaging filter to the measured Δf images. In addition, we adjusted the rotation angle of the 3D Δf image as shown in Fig. 6 in the main text.

After the data processing, we converted the Δf curves to the F curves at each xy position by the Sader's method [2]:

$$F(z) = \frac{2k}{f_0}\int_z^\infty \left(1 + \frac{a^{1/2}}{8\sqrt{\pi(t-z)}}\right)\Delta f(t) - \frac{a^{3/2}}{\sqrt{2(t-z)}}\frac{d\Delta f(t)}{dt}\,dt. \quad (1)$$

Here, k, a and f_0 denote spring constant, oscillation amplitude, and resonance frequency of the cantilever, respectively. Figure S1c shows the F curve converted from the Δf curve using Eq. (1). The Δf curve in Fig. S1c was obtained from the 3D Δf image in Fig. S1b. By repeating this force conversion at each xy position, we obtained the 3D F image as shown in Fig. S1d.

2 Calculation of Pattern Scores

In the main text, we used a method to quantitatively estimate the similarity of the pattern between two two-dimensional images. This method was used for comparing F1 and F2 slices obtained by simulations with L1-L4

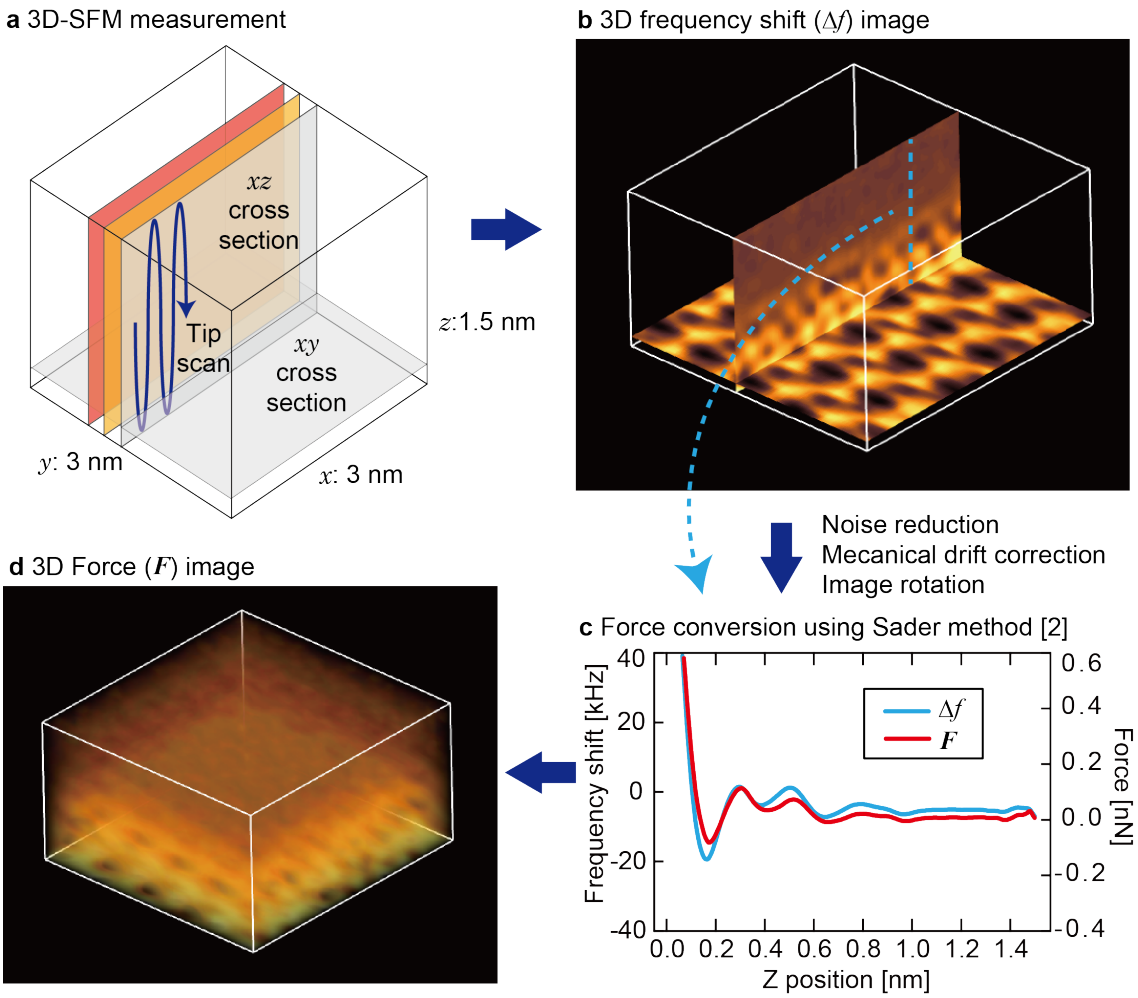

Figure S1: (a) Schematic illustration showing the principle of a 3D-SFM measurement. (b) xy and xz cross sections obtained from the 3D Δf image measured by 3D-SFM at the calcite-water interface. (c) One-dimensional (1D) conversion from a Δf curve to a F curve using the Sader's method. (d) 3D F image obtained by the force conversion from (b).

slices obtained by experiments. The obtained pattern scores are shown in Fig. 8 of the main text. Here, we describe details of the method used for this estimation.

2.1 Introduction

As Atomic Force Microscopy (AFM) experiments increase in complexity, the need for theoretical assistance becomes vital [3–8]. Usually such comparisons are done by eye, ultimately this is a very unscientific and subjective approach. Additionally making such comparisons is very difficult to justify, usually scientists will make vague statements describing a pattern (for example dot and line contrast), but quantifying and describing patterns in any more detail can become very difficult, if not impossible, for humans. This challenge is increased for the complex contrasts that appear in AFM experiments in liquids [3, 9, 10] and a more systematic image analysis approach is required.

Image recognition has been widely studied in the field of computer vision and many techniques have already been developed. Two examples are Scale-invariant feature transform (SIFT) [11] and Oriented FAST and Rotated BRIEF (ORB) [12]. Both these methods endeavour to find information dense parts of the image, referred to as keypoints. With these keypoints it is then possible to obtain a feature vector describing the image and a comparison of feature vectors can be used to generate a similarity score for two images. This has proven to be quite effective in images of real world objects, but initial testing showed that they are much less effective in AFM images due to the lack of strong contrast gradients to establish clear keypoints. Hence, we developed a method for AFM image

comparison based on the analysis of Fourier spectrums.

2.2 Fourier Transform Method

The most basic comparison of two images is a pixel by pixel comparison. Although in practice this is unlikely to obtain desirable results in AFM experiments, as knowledge of the exact location above the surface or scanning direction may not be known. Instead of using the raw pixel data, we use the Fourier transform (FT) of images – in essence the FT of an image will yield the frequency components of the image, these being unique to a particular image. In a sense, an FT of an image will produce a unique fingerprint, allowing us to use it as a convenient descriptor. Hence, by comparing various FT spectra we can gain an insight into how similar two images are. Although in order to produce a robust algorithm it is important that the spectra are insensitive to resolution, phase, scale and rotation.

2.2.1 Resolution, Scale and Phase Invariance

AFM images being compared are not necessarily going to be the same scale or resolution, hence our algorithm should be insensitive to these parameters. Luckily spatial frequencies are insensitive to size and resolution. This is easily demonstrated if one considers an image of a *sin* wave plotted over a length L and 2L as shown in Figs. S2 a and b.

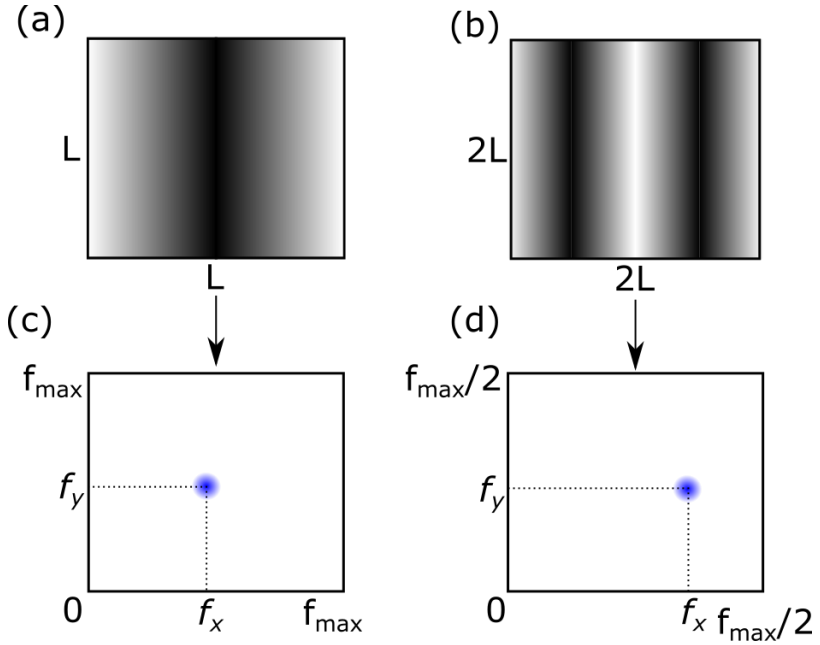

Figure S2: (a) and (b) *sin* waves of identical frequencies plotted over a distance L and 2L. (c) and (d) the FT of the corresponding *sin* wave.

A single *sin* wave would produce a single frequency in the FT (Figs. S2 c and d). If we compute the frequency values within a discrete FT, we find that upon a change in image size, the only thing that would change is the bin values and maximum/minimum frequencies. This is because only a finite range of frequencies can be represented by a discrete FT and this is a function of resolution and scale. Hence if we compute the location of the peak resulting from Figs. S2a and b we find the peak is at the same frequency value in both images (although at a different pixel position). We can exploit this to gain scale invariance, by sampling identical spatial frequencies in each image we can ensure capture of the same features independent of scale. This approach also provides spectra that are resolution invariant, since a resolution change of identical images yields the same spatial frequencies, but with different bin sizes and frequency range, similar to the difference in scale. Obtaining phase invariance is also critical since in AFM experiments the absolute position of the tip is unknown, but FT is already phase invariant if one takes the magnitude of the complex and real components of the spectrum.

2.2.2 Rotational Invariance

The scan direction of AFM images is unknown directly from an image, hence it is important that the algorithm is also insensitive to changes in rotation. This is a two step process that exploits the phase invariance already encoded into FT. We can imagine two *sin* waves, one of which is rotated by some angle, as demonstrated in Figs. S3 a and

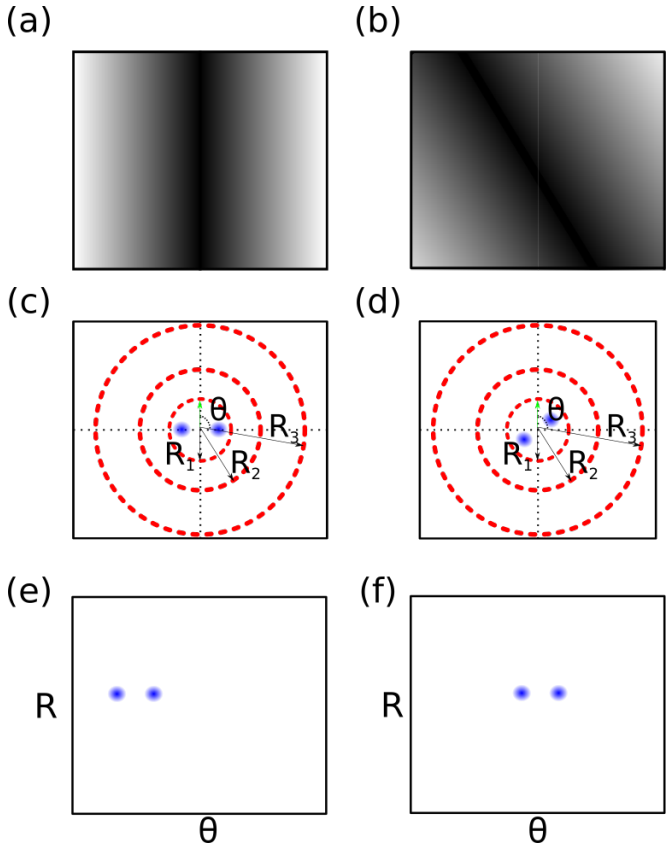

Figure S3: (a) and (b) *sin* waves of identical frequencies plotted at different angles. (c) and (d) the FT of the corresponding *sin* wave with the rotation showing in the displacement of the frequencies. (e) and (f) is polar plot being produced from c and d.

b. If we take the FT (Figs. S3 c and d) of this, we yield the same result as before (the symmetry is shown for clarity here). The rotation of the *sin* wave can be seen in the corresponding FT by a rotation of the peaks. So it is possible to represent Figs. S3 c and d in polar coordinates by simply drawing circles on our FT at varying radii. The resulting polar plot is shown in Figs. S3 e and f, as one can see the rotation is still present in this plot, although it is now represented as a phase shift. FT is insensitive to phase shifts, hence it is possible to remove this shift. However, it is important to only remove the phase shift in the θ direction, since non-rotational information is encoded into the phase of the R direction (imagine two waves of different frequencies for example). It is for this reason that we only take the one dimensional FT along the θ direction to build an array of 1D Fourier transforms.

2.2.3 Algorithm

By building upon methods discussed in sections 2.2.1 and 2.2.2 we can develop an algorithm to compare images with some reference image. The goal of this score is to produce a signal from which we can compare patterns in the image. The steps producing this are as follows:

1. Take a 2D FT of the image.
2. Take the magnitude of the FT to remove any phase shift.
3. Normalise the magnitude to remove all amplitude information.

4. Convert the previously calculated FT into polar coordinates, ensuring sampling over an equivalent area in frequency space, hence producing scale and resolution invariance.

5. Take 1D FT of each line in the polar plot to obtain a rotational invariable signal.

6. Repeat steps 1-3 for each image including the reference image.

7. For each rotational invariant signal compare it pixel by pixel with the reference and produce a score of average pixel difference between the two images.

By following the previous steps we can obtain a score of pattern similarity (PM) for each image compared to a reference image.

After completing the these processes, we obtain final score:

$$Score = 1 - exp(-PM) \tag{2}$$

This produces a normalised pattern score that is bound between 0 and 1, where 0 represents a perfect match and 1 represents the worst possible match. In the main text, we used this score for quantitatively estimating the pattern similarity between two 2D images and the results are shown in Fig. 8.

3 Pattern Scores between F Images Calculated by Simulations

Figure S4 shows the pattern scores calculated for the (a) F1 and (b) F2 slices taken from the simulated 3D F images (Fig. 4 in the main text). Focusing on the F2 slices, we find that the STA, Ca, CO_3 and OH tip produces similar contrast patterns while the OH tip provides dissimilar images to the others. In the main text, we found experimentally obtained images that are similar to those obtained by the STA, Ca and CO_3 tip models while no image was found for the OH tip model. These results consistently suggest that the OH tip model used for this study may not be realistic. This is consistent with the arguments that we made in the main text.

a F1

	Ca tip	CO_3 tip	OH tip
STA	0.949	0.961	0.923
Ca tip	0.442	0.755	
CO_3 tip	0.768		

b F2

	Ca tip	CO_3 tip	OH tip
STA	0.586	0.672	0.919
Ca tip	0.449	0.927	
CO_3 tip	0.948		

Figure S4: Pattern scores calculated for the (a) F1 and (b) F2 slices taken from the simulated 3D F images.

4 Data format of water density distribution images just under the tip

Electronic data of water density distribution images just under the tip calculated by simulations in Fig. 5(i) are available online: CaTip.txt, CO3Tip.txt and OHTip.txt.

These files are in a general text format and contain following values.

- 1st column: x position (index)
- 2nd column: y position (index)
- 3rd column: x position (unit: [nm])
- 4th column: y position (unit: [nm])
- 5th column: water density (unit: [nm^{-3}])

References

[1] K. Miyazawa, N. Kobayashi, M. Watkins, A. L. Shluger, K. Amano, and T. Fukuma, "A relationship between three-dimensional surface hydration structures and force distribution measured by atomic force microscopy," *Nanscale*, vol. 8, p. 7334, 2016.

[2] J. E. Sader and S. P. Jarvis, "Accurate formulas for interaction force and energy in frequency modulation force spectroscopy," *Appl. Phys. Lett.*, vol. 84, pp. 1801–1803, 2004.

[3] K. Miyata, J. Tracey, K. Miyazawa, V. Haapasilta, P. Spijker, Y. Kawagoe, A. S. Foster, K. Tsukamoto, and T. Fukuma, "Dissolution processes at step edges of calcite in water investigated by high-speed frequency modulation atomic force microscopy and simulation," *Nano Letters*, vol. 17, no. 7, pp. 4083–4089, 2017. PMID: 28650174.

[4] G. H. Enevoldsen, H. P. Pinto, A. S. Foster, M. C. R. Jensen, W. A. Hofer, B. Hammer, J. V. Lauritsen, and F. Besenbacher, "Imaging of the Hydrogen Subsurface Site in Rutile TiO_2," *Phys. Rev. Lett.*, vol. 102, p. 136103, Apr 2009.

[5] A. S. Foster, C. Barth, and C. R. Henry, "Chemical Identification of Ions in Doped NaCl by Scanning Force Microscopy," *Phys. Rev. Lett.*, vol. 102, p. 256103, Jun 2009.

[6] P. Spijker, T. Hiasa, T. Musso, R. Nishioka, H. Onishi, and A. S. Foster, "Understanding the Interface of Liquids with an Organic Crystal Surface from Atomistic Simulations and AFM Experiments," *The Journal of Physical Chemistry C*, vol. 118, no. 4, pp. 2058–2066, 2014.

[7] R. Bechstein, C. González, J. Schütte, P. Jelínek, R. Pérez, and A. Kühnle, "'All-inclusive' imaging of the rutile TiO_2 (110) surface using NC-AFM," *Nanotechnology*, vol. 20, no. 50, p. 505703, 2009.

[8] L. Gross, F. Mohn, N. Moll, P. Liljeroth, and G. Meyer, "The Chemical Structure of a Molecule Resolved by Atomic Force Microscopy," *Science*, vol. 325, no. 5944, pp. 1110–1114, 2009.

[9] J. Tracey, K. Miyazawa, P. Spijker, K. Miyata, B. Reischl, F. F. Canova, A. L. Rohl, T. Fukuma, and A. S. Foster, "Understanding 2D atomic resolution imaging of the calcite surface in water by frequency modulation atomic force microscopy," *Nanotechnology*, vol. 27, no. 41, p. 415709, 2016.

[10] B. Reischl, P. Raiteri, J. D. Gale, and A. L. Rohl, "Can Point Defects in Surfaces in Solution be Atomically Resolved by Atomic Force Microscopy?," *Phys. Rev. Lett.*, vol. 117, p. 226101, Nov 2016.

[11] D. G. Lowe, "Object Recognition from Local Scale-Invariant Features," *Corfu*, 1999.

[12] E. Rublee, V. Rabaud, K. Konolige, and G. Bradski, "ORB: An efficient alternative to SIFT or SURF," in *2011 International Conference on Computer Vision*, pp. 2564–2571, IEEE, nov 2011.